

The Role of Carbon in Grain Refinement of Cast CrFeCoNi High-Entropy Alloys



X.W. LIU, L. LIU, G. LIU, X.X. WU, D.H. LU, J.Q. YAO, W.M. JIANG, Z.T. FAN,
and W.B. ZHANG

As a promising engineering material, high-entropy alloys (HEAs) CrFeCoNi system has attracted extensive attention worldwide. Their cast alloys are of great importance because of their great formability of complex components, which can be further improved through the transition of the columnar to equiaxed grains and grain refinement. In the current work, the influence of C contents on the grain structures and mechanical properties of the as-cast high-entropy alloy CrFeCoNi was chosen as the target and systematically studied *via* a hybrid approach of the experiments and thermodynamic calculations. The alloys with various C additions were prepared by arc melting and drop cast. The as-cast macrostructure and microstructure were characterized using optical microscopy, scanning electron microscopy, and transmission electron microscopy. The cast HEAs transform from coarse columnar grains into equiaxed grains with the C level increased to ≥ 2 at. pct and the size of equiaxed grains is further decreased with the increasing C addition. It is revealed that the interdendritic segregation of Cr and C results in grain boundary precipitation of $M_{23}C_6$ carbides. The grain refinement is attributed to the additional constitutional supercooling from the C addition. The yield stress and tensile strength at room temperature are improved due to the transition of columnar to equiaxed grains and grain refinement.

<https://doi.org/10.1007/s11661-018-4549-8>

© The Minerals, Metals & Materials Society and ASM International 2018

I. INTRODUCTION

HIGH-ENTROPY alloys (HEAs), also referred to multicomponent alloys or compositionally complex alloys, have attracted extensive attention during the past decade due to their unique properties.^[1] As proposed firstly by Yeh,^[2] HEA is defined as an alloy containing at least five principal elements, each with an atomic percentage between 5 and 35 pct. This definition is extended to the equiatomic quaternary alloys^[3–6] with FCC or BCC structure afterwards, since they also have high mixing entropy, and even higher than some non-equiatomic quinary HEAs.^[7–9] Therefore, we also

use this generalized category in the present work. Among these alloys, face-centered cubic (FCC)-based HEAs, especially CrFeCoNi family alloys, were investigated systematically and shown exceptional room temperature and cryogenic mechanical properties.^[10–27] Meanwhile, another unique characteristic of HEAs is the absence of “solvent” and “solute” atoms, resulting in a breakdown of the traditional textbook theory that the solutes redistribute during solidification. Therefore, they have more different solidification behaviors compared with the traditional compositionally simple alloys.

Casting is a very important technique for almost all the engineering materials to form extremely complicated and thin components. However, the other techniques, such as machining and forging, are only suitable for the relatively simple-shaped components. Even for some FCC alloys with good ductility, *e.g.*, Cu and Al alloys, cast alloys are still required in many cases. Therefore, the casting technique for the above-mentioned FCC HEAs is of importance for applications. In the fields of cast alloys, microstructure control and grain refinement are two of the most importance issues, since the general cast alloys are inclined to grow along the heat flow direction and form bulky columnar gains. These coarse columnar grains lead to two typical shortcomings. Firstly, these grains are generally very coarse with hundreds of micrometers thickness or more. For

X.W. LIU, W.M. JIANG, Z.T. FAN, L. LIU, D.H. LU, and J.Q. YAO are with the State Key Laboratory of Materials Processing and Die & Mould Technology, Huazhong University of Science and Technology, Wuhan, China and also with the State Key Laboratory of Solidification Processing, Northwestern Polytechnical University, Xi'an, China. G. LIU is with the School of Material Science and Engineering, Xi'an University of Technology, Xi'an 710048, China. X.X. WU is with the Institute for Materials, Ruhr University Bochum, 44801 Bochum, Germany. W.B. ZHANG is with the Institute for Applied Materials—Applied Materials Physics, Karlsruhe Institute of Technology, 76344 Eggenstein-Leopoldshafen, Germany. Contact e-mails: fanzt@hust.edu.cn and weibin.zhang@kit.edu

Manuscript submitted October 17, 2017.

Article published online March 12, 2018

example, some cast Al alloys could form columnar grains with the thickness of more than 1 mm.^[28] This type of coarse columnar grains also occurs in the as-cast microstructure of HEAs, *e.g.*, as-cast CrMnFeCoNi HEAs,^[16] leading to the relatively low strength.^[29] Columnar grains result in anisotropic mechanical properties in different loading directions and limit the engineering applications under complex service stresses. Transition from columnar to equiaxed grains can improve the isotropy of the microstructure and optimize the mechanical properties. Secondly, the coarse grains in as-cast state lead to the poor mechanical properties. According to the Hall–Petch relationship, the strengthening of HEAs by grain refinement has been proved by many researchers^[11,30] mainly through the cold deformation and recrystallization. However, almost no one investigated the grain refinement of cast HEAs systematically until now.

There are many methods for the grain refinement of traditional solid solution alloys,^[31] and solute effect related to constitutional supercooling during solidification is one of the most commonly used techniques. For the compositionally simple alloys, *e.g.*, diluted binary solid solution alloys, the solute is rejected sideways ahead of solid–liquid interface during solidification. The solute-enriched zone leads to the constitutional supercooling, which restricts the growth of growing solid–liquid interface or even induces nucleation depending on its extent, leading to the grain refinement.^[32] The formation of dendrites in alloys is often attributed to the constitutional supercooling.^[33] Actually, HEAs still form dendrites inside the columnar grains during solidification, although no clear “solute” and “solvent” could be distinguished. Laurent-Brocq *et al.*^[22] studied the solidified microstructure of CrMnFeCoNi HEA, and found that dendrites are enriched in Co, Cr, and Fe, whereas interdendrites are enriched in Mn and Ni. However, coarse columnar grains still form in the as-cast CrMnFeCoNi HEA,^[16] which means that the constituent supercooling, even if existing, is not sufficient enough for grain growth restriction. Considering the other grain refinement methods, *i.e.*, adding grain refiners or imparting external force fields, they are difficult to be conducted in the commonly used cast technique compared to the solute effect. From this viewpoint, generating a sufficient degree of additional constitutional supercooling is required to induce columnar to equiaxed grain transition and further grain refinement. This is often achieved through the compositional modification, *i.e.*, alloying.

In this study, equiatomic CrFeCoNi HEA was selected as the base alloy to investigate the effect of C addition on columnar to equiaxed grain transition and grain refinement of their as-cast microstructures. Although some researchers have studied the effect of C addition on the microstructures and mechanical properties of HEAs,^[5,8,34,35] they did not focus on the grain refinement of the cast alloys. Various contents of C were added to study systematically the evolution of columnar to equiaxed grain transition and grain sizes. The tensile properties at room temperature were tested. The mechanism of grain refinement of cast alloys was also discussed.

II. EXPERIMENTAL

A. Ingot Preparation

CrFeCoNi- x at. pct C ($x = 0-3$) HEA ingots were prepared by arc melting a mixture of pure metals of Cr, Fe, Co, and Ni (purity > 99.5 wt pct) and Cr₃C₂ powders (purity > 99 wt pct) in a high-purity argon atmosphere. The contents of matrix elements Cr, Fe, Co, and Ni are always equiatomic and the compositions are written as CrFeCoNi- x C or x C HEA for short hereafter. After the raw materials were loaded in the arc melter, the chamber was first evacuated to $\sim 5 \times 10^{-2}$ Pa, then backfilled with pure Ar, followed by evacuating twice to dilute the residual air inside the chamber, and finally backfilled at a pressure of $\sim 5 \times 10^4$ Pa. Before the materials were melted, a small piece of pure Ti was melted to get any residual oxygen or nitrogen that might be present in the chamber. Additionally, the Cr₃C₂ powders were stacked between the other constituents to minimize loss. The buttons were remelted and flipped five times to ensure chemical homogeneity before they were drop cast into a rectangular copper mold with the dimensions of $8 \times 17 \times 70$ mm³.

B. Microstructure Characterization

The lower half part of the ingots was investigated here, since this part has relatively similar solidification conditions and kept a necessary distance from the riser. The ingots were firstly cut by electric discharge machining (EDM) from the cross sections 30 mm away from the bottom, where a similar solidification condition could be expected for intercomparison. The microstructures of the cross sections were observed by SEM. Meanwhile, the lower part was cut vertically parallel to the short wall, where the vertical section was observed by optical microscope (OM) to obtain the macrostructure. The drop-cast ingot and the positions for observation are schematically shown in Figure 1. SEM specimens were initially polished to 2500-grit SiC paper and electrochemically polished for the final surface clarification using an electrochemical polishing machine (Struers TenuPol-5) with a direct voltage of 50 V at room temperature. The electrolyte is composed of 90 vol

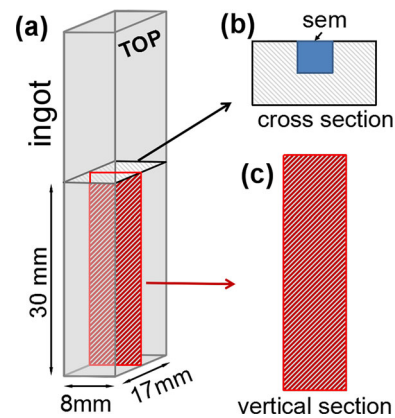


Fig. 1—Schematic drawings showing: (a) drop-cast HEA ingot, the cross section (b) for SEM observation and vertical section (c) for OM observations.

pct methyl alcohol and 10 vol pct HClO_4 . The microstructures were examined using a Zeiss AURIGA FIB-SEM equipped with an energy dispersive X-ray spectroscopy (EDX) X-Max^N from Oxford Instruments at an accelerating voltage of 20 kV. Grain sizes were measured with the linear intercept method outlined in ASTM E112-10. Elongation factor (E), which describes the degree of dimensional isotropy of a grain, is defined as the ratio of the longest dimension to the smallest dimension of a grain.^[36] For convenience, the elongation factor (E) value is used as the critical value to distinguish the equiaxed and columnar grains in the current work. The grains were defined as columnar grains when the E was larger than 2, otherwise defined as equiaxed grains. The vertical sections were initially polished to 2500-grit SiC paper and then etched by a corrosive liquid composed of hydrochloric acid (10 mL) and picric acid (2 g) for 30 seconds. Their macrostructures were observed by a Zeiss Stemi 2000 stereoscope. The phase characterization was carried out by X-ray diffraction using a Shimadzu XRD-7000S diffractometer (working voltage = 40 kV, current = 20-30 mA, Cu $K\alpha$ radiation $\lambda = 0.154$ nm; 2θ -range from 20 to 80 deg, scanning rate = 3 deg/min.). The specimen for TEM analysis was firstly ground to a thickness of ~ 70 μm , and then prepared by twin-jet electron chemical thinning at 40 V using a mixture consisting of 90 vol pct glacial acetic acid and 10 vol pct HClO_4 at room temperature. TEM investigations were performed using JEM-2100 F microscope operated at an accelerating voltage of 200 kV.

III. RESULTS

A. Macrostructure Evolution

The macrostructures of vertical sections of cast CrFeCoNi- x C HEAs ($x = 0, 1, 1.5, 2, 2.5,$ and 3 at.

pct) are shown in Figure 2. As can be seen, baseline CrFeCoNi HEA has long columnar grains growing from the wall to the center (Figure 2(a)). With the addition of C (below 1.5 pct), obvious columnar to equiaxed transition can occur, and the widths and lengths of the coarse columnar grains seem becoming reduced as compared with the baseline HEA, as illustrated in Figures 2(b) and (c). Figures 2(e) through (f) show that only the uniform and fine equiaxed grains can be observed once the C concentration exceeded 2 at. pct, but the grain size cannot be distinguished from the macrostructural image. Note that the shrinkage porosities (indicated by the red circles) can form in all the alloys. The samples with columnar grains are likely to form visible shrinkage porosities, which rarely appear after the structures transform to equiaxed grains. However, the reduction of shrinkage porosity by grain refinement was also indicated by other work.^[37]

B. Microstructures

For clarity, SEM BSE was conducted to further observe the microstructure of the cross sections in the cast CrFeCoNi- x C ($x = 0, 1, 1.5, 2, 2.5,$ and 3 at. pct), as shown in Figure 3. A few pores are visible in all the images. They appear to be casting porosity and/or holes left over from particles that fell out during the polishing process, which was also found in the similar materials.^[12,38] From these figures, it can be seen more clearly that the addition of C produces a dramatic grain refining effect in the CrFeCoNi HEA, indicating that C is an effective grain refiner. After a small addition of C (≤ 1.5 at. pct), coarse columnar grains are still visible. However, when the C level is increased to above 2 at. pct, the columnar grains are suppressed and equiaxed grains almost occupy the whole samples. For the critical C addition of 2 pct, it is found that the grain sizes are fluctuated throughout the sample. With more C addition

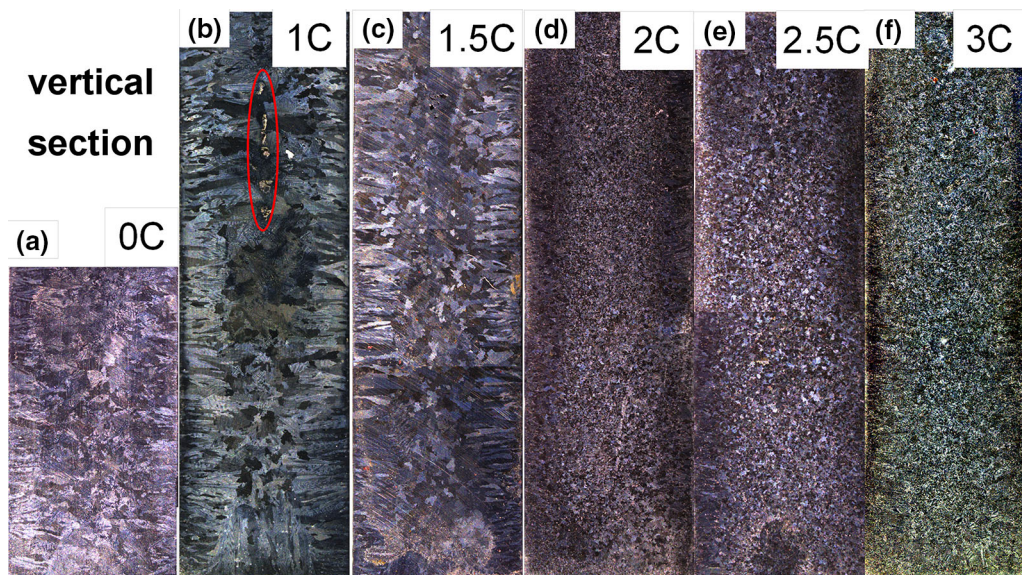


Fig. 2—Macrographs of vertical sections of cast CrFeCoNi- x at. pct C with $x = 0$ (a), 1 (b), 1.5 (c), 2 (d), 2.5 (e), and 3 (f). Note that the width of samples is all 8 mm.

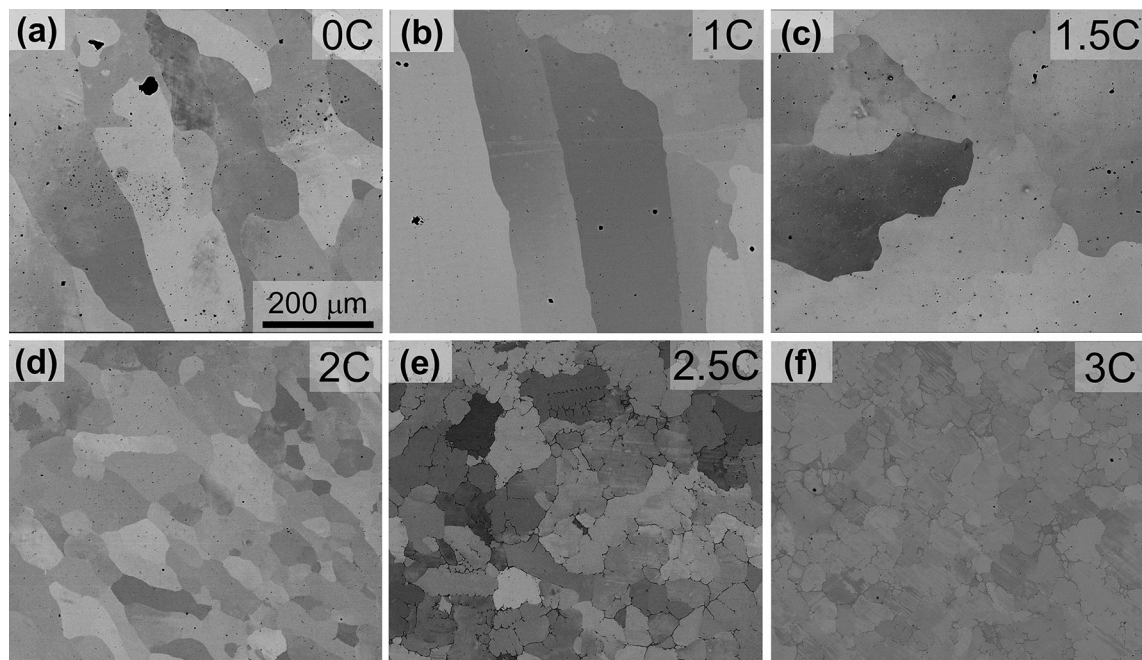


Fig. 3—SEM BSE images of the cross sections of CrFeCoNi- x at pct C with $x = 0$ (a), 1 (b), 1.5 (c), 2 (d), 2.5 (e), and 3 (f).

(≥ 2 at. pct), the equiaxed grain sizes distribute almost uniformly, and even in the edge part of the samples. Moreover, there are some precipitates in the grain boundaries of the HEAs with high level C, which will be further discussed in the following section. Grain sizes were measured with the linear intercept method outlined in ASTM E112-10. As mentioned in the experimental procedure, the mean grain size was obtained by measuring three different regions of the sample, since there was variation of grain size from the center to the edge as a result of differences of the cooling rate. In this case, grain size was measured using the width of the columnar grains. The plot of grain size vs C addition is shown in Figure 4, in which the alloys with columnar grains are marked by solid circles and expressed with the width of the columnar grains, whereas the alloys with equiaxed grains are marked by solid squares with mean grain diameters. It is clearly observed that the equiaxed grain size decreases with the increasing C addition. The average columnar grain widths, while the equiaxed grain size decreases gradually with a further C addition up to 3 pct.

Enlarged SEM BSE images of the CrFeCoNi and CrFeCoNi-3C HEAs are shown in Figure 5, respectively. From the images, it can be seen that the grain boundaries of the CrFeCoNi HEA are smooth and no precipitate is present there. However, there are some lamellar structure with the thickness of less than one micron along the grain boundaries in the CrFeCoNi-3C HEA, exhibited as dark contrast. A line across the precipitate lamella was selected in Figure 5(b) for the EDX line scanning, and three points marked by red spot were chosen for compositional analysis (as summarized in Table I). The composition in matrix (point 1) is similar to the nominal composition. However, the lamella region (point 2) has more Cr and C, and further

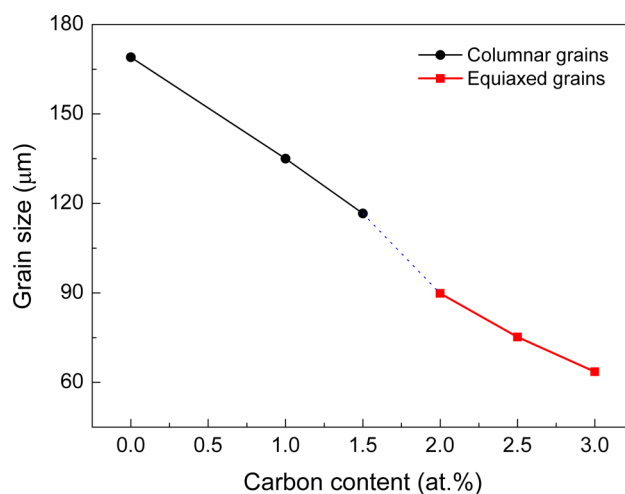


Fig. 4—Plots of measured grain size vs. carbon content of CrFeCoNi- x C HEAs, where the columnar-grained HEAs were measured by the mean width of columnar grains and the equiaxed-grained HEAs by the mean diameter of equiaxed grains.

the dark lath in triangle grain boundaries (point 3) shows clear enrichment of Cr and C. The dark lath in point 2 has a thickness of less than 1 micron, and thus its EDX composition also contains the sideward bright lath. Consequently, the dark precipitates around grain boundaries are carbides, which will be further identified by TEM analysis.

The EDX elemental maps of the CrFeCoNi and CrFeCoNi-3C HEAs are shown in Figure 6, respectively. As expected, the two cast HEA alloys exhibit some composition fluctuations at a micrometer scale after drop cast because of the solute redistribution during solidification. Although the CrFeCoNi alloy has

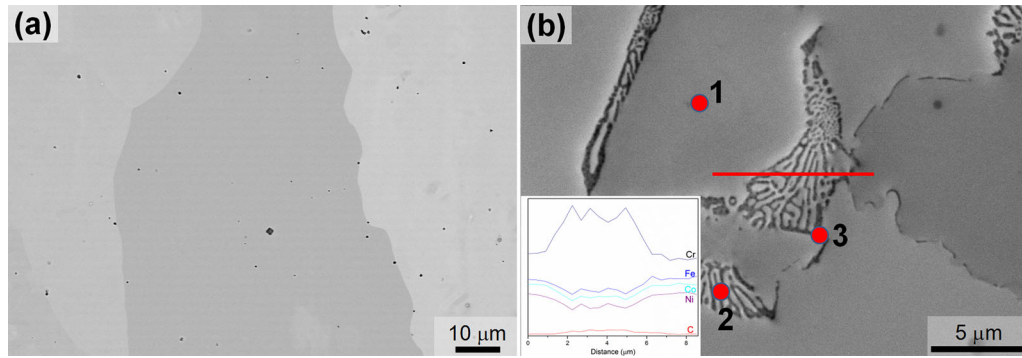


Fig. 5—Enlarged SEM BSE images of CrFeCoNi (a) and CrFeCoNi-3C (b) HEAs, where a line across the precipitate lamella was selected in the latter for the EDX line scanning whose results are attached in the lower left inset, and three positions marked by red points were chosen for elemental analysis whose results are summarized in Table I (Color figure online).

the columnar grains from BSE, it shows a dendritic-like morphology inside. The dendrites are enriched in Fe, Co, and Ni, whereas the interdendritic areas are enriched in Cr (Figure 6(a)). However, the elemental fluctuations in dendrites are not coincident with the grain boundaries. As for the CrFeCoNi-3C HEA alloy, the elemental fluctuations are different from the baseline CrFeCoNi HEA. Because of the formation of equiaxed grains induced by C addition, the dendrite morphologies inside the grains are not distinct as those in the baseline alloy. In this case, the elemental fluctuations occur in the grain boundaries, *i.e.*, Cr and C are enriched in the grain boundaries, whereas Fe, Co, and Ni are enriched in the intragains. Therefore, grains' refinement by C addition changes the microstructural morphologies and solute fluctuations simultaneously.

In order to understand the phase constituents with the addition of C, the as-cast CrFeCoNi- x C ($x = 0, 2.5$ and 3) HEA samples were examined by XRD analysis. After indexing the diffraction spectra (Figure 7), it can be seen that the spectrums show only the peaks of single FCC phase, indicating that these two C-containing samples contain the same phases with baseline CrFeCoNi HEA. One has to be aware that only one phase in XRD pattern cannot unambiguously confirm the real single phase in the alloy. Indeed, phases with a low volume fraction, typically lower than 5 pct, cannot be detected by XRD.^[22] The phase constituent needs to be characterized further.

Transmission electron microscopy (TEM) was used to characterize the detailed microstructure and phase constituents of the C-containing HEA. As an example, the TEM image of the CrFeCoNi-2C HEA is shown in Figure 8. Figure 8(a) shows a typical low-magnification TEM image, in which some precipitates in the grain boundaries with a thin ribbon-like morphology are clearly observed. Most of the precipitates have straight sides and discontinuous structure, as shown in Figure 8(b). The corresponding dark-field image of the precipitates, as shown in Figure 8(c), confirms the different crystal structure with a thickness of about 200 nm. In more detail, the selected area electron diffraction pattern of the precipitate in Figures 8(b) and (c) is illustrated in Figure 8(d) and was indexed to

Table I. Chemical Compositions of the Precipitates and Matrix (At. Pct) in CrFeCoNi-3C High-Entropy Alloy Measured by SEM EDX

Point (Position)	Cr	Fe	Co	Ni	C
1 (matrix)	21.89	20.56	21.00	21.34	15.21
2 (lamella)	32.18	16.04	15.80	14.53	21.45
3 (precipitate)	38.51	11.96	10.71	08.35	30.47

be $M_{23}C_6$ carbides. These kinds of carbides mainly consist of Cr and C, but also contain some other constituents, like Fe, Co, and Ni. This is consistent with the EDX results of C-containing HEAs (Figure 6(b)).

C. Mechanical Properties at Room Temperature

The tensile properties were tested at room temperature, as shown in Figure 9. Figure 9(a) shows representative engineering stress–strain curves for the CoCrFeNi- x C ($x = 0, 2, 2.5, 3$) materials. The other low-C HEAs are not shown here because of their undesirable columnar grains. Figure 9(b) summarizes the C content dependency of the 0.2 pct offset yield strength σ_y , ultimate tensile strength σ_u , and elongation to fracture ϵ_f . Both the strengths and the ductility show strong dependencies of C addition. The addition of C results in a significant enhancement of the tensile strength, especially yield strength. For instance, the yield strength of equiaxed-grained CoCrFeNi-3C HEA (~ 335 MPa) is increased by ~ 100.6 pct compared with the baseline CoCrFeNi HEA (~ 167 MPa). The elongation to fracture, however, is decreased with the addition of C, but is still quite high.

IV. DISCUSSION

The microstructural analyses using multiple complementary techniques (OM, SEM, TEM, EDX, and SAD) have shown that the C addition could induce the columnar to equiaxed grain transition and grain refinement of the CrFeCoNi HEA, which were produced by commonly used arc melting and drop casting. The

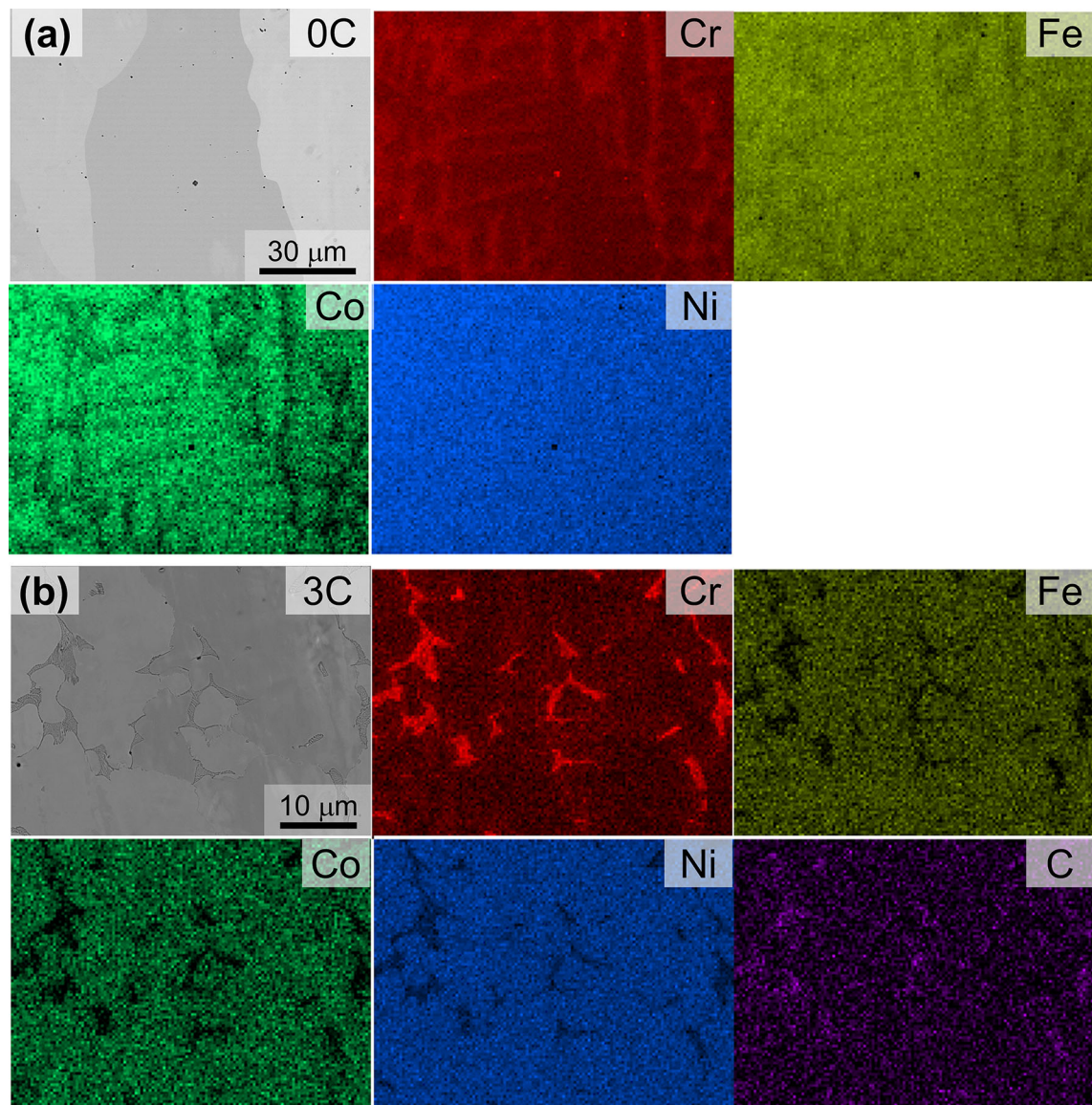


Fig. 6—SEM EDX maps of CrFeCoNi (a) and CrFeCoNi-3C (b) HEAs.

columnar grains remain with the C addition of < 2 at. pct, while equiaxed grains form with the C addition of ≥ 2 at. pct. The tensile properties of CrFeCoNi-2C, CrFeCoNi-2.5C, and CrFeCoNi-3C are very similar, but the strengths are increased significantly compared with the baseline CrFeCoNi HEA. Given that the grain size distribution of CrFeCoNi-2C is not as uniform as the latter two materials, 2.5 and 3 C were considered as the appropriate additions for this HEA. This C-induced grain refinement of CrFeCoNi HEA will be discussed in detail.

Nucleant-particle theory (or called heterogeneous nucleation) has been the most popular method for grain refinement of alloys.^[39–41] In this study, we did not find any intragranular particles. If the heterogeneous nucleation is induced by in-site particles, these particles should be observed inside the grains. For instance, adding C to Mg-Al alloys, Al_4C_3 could precipitate in the liquid and act as the heterogeneous nucleation sites to

refine the grains significantly.^[42,43] However, only carbides along the grain boundaries have been observed in our alloys (Figure 8). These lamellae carbides could not act as the heterogeneous sites, but may retard the grain growth during the solidification processing. In order to clarify this issue, pseudo-binary phase diagram of CrFeCoNi-C system is calculated by Thermo-Calc software based on the database of TCFE7, where the CrFeCoNi is always kept equiatomic, as shown in Figure 10. From the phase diagram, we can see that M_7C_3 carbides form after solidification. Although M_{23}C_6 carbides are observed, the initial carbides are M_7C_3 carbides at high temperature which transform into M_{23}C_6 during the subsequent cooling process. The sigma phase is also present in the phase diagram. However, it could not form during fast cooling of ingots. One needs to be aware that the phase diagram is calculated under an equilibrium condition. These equilibrium phases, *e.g.*, sigma, could precipitate during a

long anneal.^[38] In the viewpoint of crystal growth, the carbides present here could not refine the solidification grains. Combining with the XRD, SEM, and TEM results, one can conclude that the enrichment regions of C and Cr ahead of the solid-liquid interface begin to decompose into two phases under a eutectic reaction, which was also observed by other researchers.^[26,27,44]

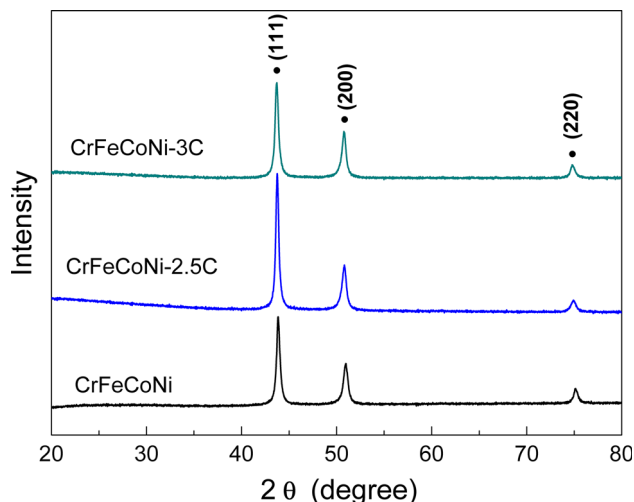


Fig. 7—XRD patterns of CrFeCoNi-C ($x = 0, 2.5,$ and 3 at. pct) HEAs.

The diffusion behavior of constituent elements during solidification has been influenced by the addition of C, which is indicated by Figure 6. Moreover, the carbides indexed in TEM (Figure 8) indicated the enrichment of C and Cr in the grain boundaries, *i.e.*, solid-liquid interface during solidification. Thus, it is considered that the grain refinement is caused by the action of solutes, especially C. The effect of solutes on grain refinement has been proved by many researchers.^[32,45-47] The effect has been investigated in various Al alloy systems and explained in terms of the growth restriction factor (GRF). Addition of solute elements generates constitutional undercooling in a diffusion layer ahead of the advancing solid/liquid interface, which restricts grain growth since the solute diffuses slowly, and thus limits the rate of crystal growth. GRF, designated Q , is defined as $m_L c_0 (k - 1)$.^[48] Here, Q could not be obtained from the phase diagram since there is an interval of melting points of the matrix (Figure 10). However, one can see from the phase diagram that the solute of C has a partition coefficient of $k < 1$, which means that C is rejected ahead of the solid-liquid interface during solidification. This is in agreement with the SEM EDX (Figure 5) and TEM analysis (Figure 8). The enrichment of C in front of the solid-liquid interface could produce additional constitutional supercooling, which depends on its content and partition coefficient. Besides, the addition of C also facilitates elemental build-ups of Cr ahead of the advancing solid-liquid interface. Such

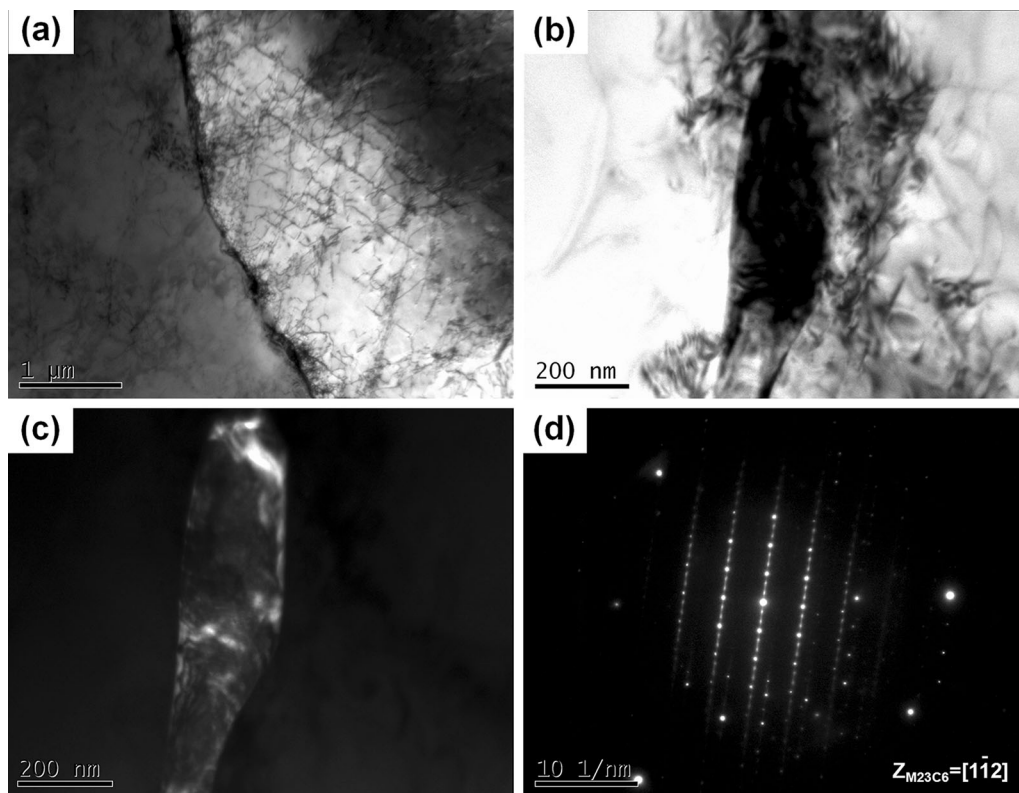


Fig. 8—TEM images of CrFeCoNi-2C HEA. (a) Typical grain boundary containing precipitates. (b) and (c) are bright-field image and corresponding dark-field image of precipitates in the grain boundaries, respectively. (d) Selected area electron diffraction pattern of precipitate, showing that it is carbide.

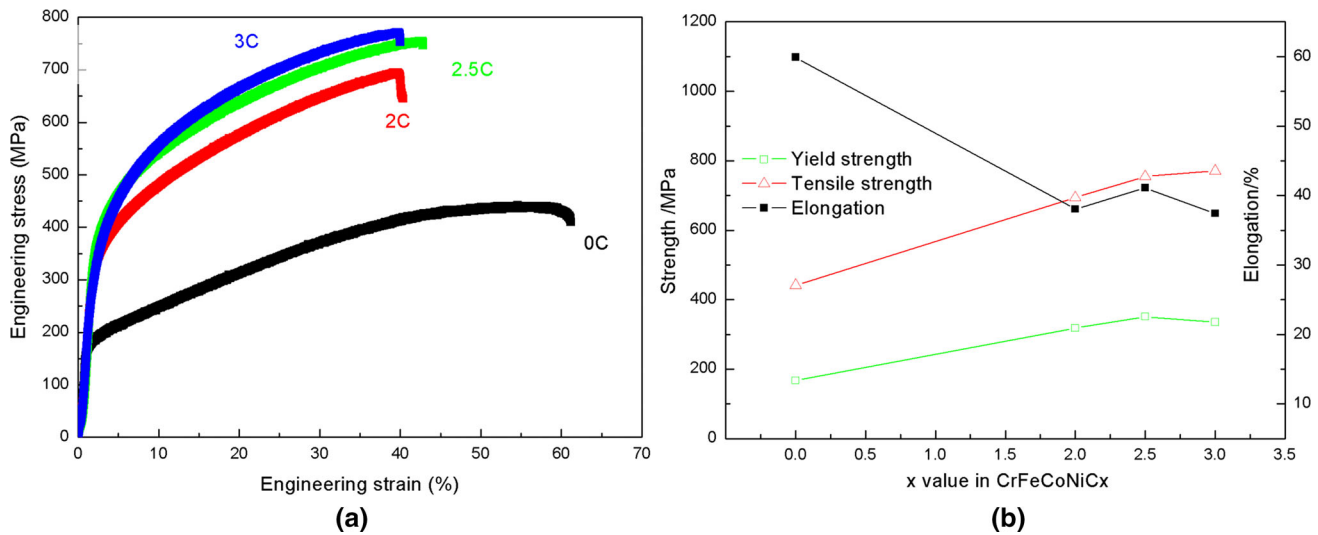


Fig. 9—(a) Representative engineering stress–strain curves of the CoCrFeNi- x at pct C ($x = 0, 2, 2.5, 3$) alloys at room temperature, where the C addition is marked next to the corresponding curve. (b) Dependence of the tensile strength, yield strength, and elongation on the C addition.

build-ups generate constitutional supercooling in the diffusion layer in front of the interface, locally reducing the nucleation barrier for crystallization and further resulting in finer grains. The grain refinement by C addition was also found in many alloys, which is caused by solute-induced additional constitutional supercooling but not by heterogeneous nucleation. For example, Yamanaka^[49] found that C produces great grain refinement in Co-28Cr-9W-1Si alloys and attributed this to the effect that C facilitates elemental build-ups ahead of the advancing solid–liquid interface.

The tensile properties of the CrFeCoNi-C HEAs at room temperature are improved significantly due to the microstructural optimization and grain refinement, which could be seen from Figure 9. The enhancement of strength does not lose too much of the elongation. It is noted that the microstructural change here includes not only the grain morphology and size, but also the phase constituents, *i.e.*, ultrafine carbide precipitate in the grain boundaries. It could not be ignored that the precipitates in grain boundaries improve the effect of grain boundaries as obstacles of dislocation during deformation. Wu *et al.*^[12] studied the deformation behavior of CrFeCoNi HEAs and indicated that these alloys comply with Hall–Petch relationship at room temperature, where the formula could be deduced from their data as $\sigma_y = 94.8 \text{ (MPa)} + 853.4 \text{ (MPa} \cdot \mu\text{m}^{1/2}) D^{-1/2} \text{ (}\mu\text{m}^{-1/2})$. According to this formula, for example, the yield strength of CrFeCoNi-3C alloy should be 201.5 MPa. However, the tested yield strength of the material is 335.2 MPa. The increment of yield strength between tested value and calculated one according to Hall–Petch relationship is much higher than the portion resulted from the reduced grain size. Therefore, the excessive part should be ascribed to carbide precipitates in grain boundaries. It should be noted that the tested yield strength (167.3 MPa) of current cast CrFeCoNi is very similar to the calculated value (160.4 MPa) from the above Hall–Petch formula. In addition, the

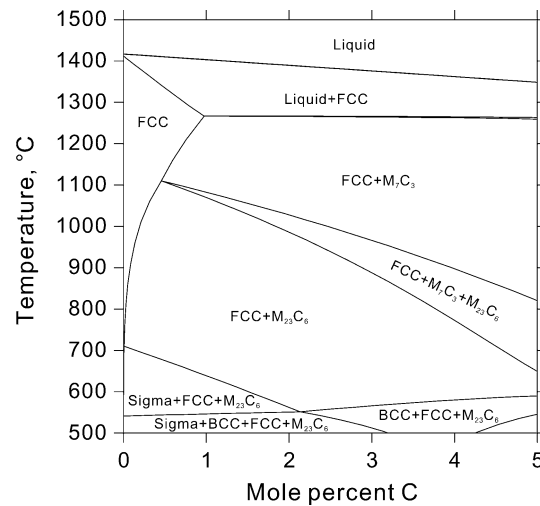


Fig. 10—Pseudo-binary phase diagram of CrFeCoNi-C system, calculated by Thermo-Calc software with the database of TCFE7, where the CrFeCoNi is always kept equiatomic.

transition of columnar to equiaxed grains also leads to isotropy, which is very important for the industrial application under polydirectional loads. However, this could not be reflected in the tensile properties. Furthermore, the elongation is decreased after addition of C, which occurs commonly in the alloys with precipitates. However, the loss of elongation is not so high, *i.e.*, the high-C CrFeCoNi-3C HEA still has a quite high value (~37 pct) and meets the practical requirement well.

V. CONCLUSIONS

Various content of C was added into the cast CrCoFeNi high-entropy alloys to investigate its effect on the structures and mechanical properties of HEA by integrating the experiments and calculations. The alloys

were produced by arc melting and drop casting. Their microstructures, elemental distribution, and phase constituents after solidification were examined and related tensile properties were tested. According to the thermodynamic calculation, the grain refinement mechanism was interpreted. Based on our observations, the following conclusions can be drawn.

- (1) The cast CrCoFeNi high-entropy alloy has coarse columnar grains. After adding a small amount of C (≤ 1.5 at. pct), coarse columnar grains are still visible. However, when the C level is increased to ≥ 2 at. pct, the columnar grains transform into equiaxed grains. The grain size is decreased gradually with the increasing addition of C.
- (2) The cast CrCoFeNi high-entropy alloy is a single FCC alloy. After C addition, $M_{23}C_6$ carbides precipitate along the grain boundaries to form as eutectic-like lamellae.
- (3) Dendrite morphology exists inside the columnar grains of CrFeCoNi alloy, where the dendrites are enriched in Fe, Co, and Ni, whereas the interdendritic areas are enriched in Cr. However, Cr and C are enriched in grain boundaries, whereas Fe, Co, and Ni are enriched in the intragrain for the equiaxed alloy with C addition.
- (4) With the C addition, the yield stress and tensile stress at room temperature are increased, whereas the elongation is decreased, but still retains a quite high value.
- (5) The grain refinement with the C addition is attributed to the effect that carbon facilitates elemental build-ups ahead of the advancing solid-liquid interface and generates additional constitutional supercooling.

ACKNOWLEDGMENTS

The authors would like to thank the support of the National Nature Science Foundation of China (51775204, 51301123, 51604222 and 51204073), the opening fund (SKLSP201711) of State Key Laboratory of Solidification Processing in NWPU, and the Analytical and Testing Center, HUST.

REFERENCES

1. Y. Zhang, T.T. Zuo, Z. Tang, M.C. Gao, K.A. Dahmen, P.K. Liaw, and Z.P. Lu: *Prog. Mater. Sci.*, 2014, vol. 61, pp. 1–93.
2. J.W. Yeh, S.K. Chen, S.J. Lin, J.Y. Gan, T.S. Chin, T.T. Shun, C.H. Tsau, and S.Y. Chang: *Adv. Eng. Mater.*, 2004, vol. 6 (5), pp. 299–303.
3. J.Y. He, H. Wang, H.L. Huang, X.D. Xu, M.W. Chen, Y. Wu, X.J. Liu, T.G. Nieh, K. An, and Z.P. Lu: *Acta Mater.*, 2016, vol. 102, pp. 187–96.
4. H. Huang, Y. Wu, J. He, H. Wang, X. Liu, K. An, W. Wu, and Z. Lu: *Adv. Mater.*, 2017, vol. 29 (30), pp. 1701678.
5. T. Huang, L. Jiang, C. Zhang, H. Jiang, Y. Lu, and T. Li: *Science China Technological Sciences*, 2017.
6. H.W. Yao, J.W. Qiao, M.C. Gao, J.A. Hawk, S.G. Ma, H.F. Zhou, and Y. Zhang: *Mater. Sci. Eng. A*, 2016, vol. 674, pp. 203–11.
7. D. Ma, M. Yao, K.G. Pradeep, C.C. Tasan, H. Springer, and D. Raabe: *Acta Mater.*, 2015, vol. 98, pp. 288–96.
8. S. Fang, W. Chen and Z. Fu: *Mater. Design*, 2014, vol. 54 (Supplement C), pp. 973–79.
9. D.G. Shaysultanov, G.A. Salishchev, Y.V. Ivanisenko, S.V. Zhrebtsov, M.A. Tikhonovsky, and N.D. Stepanov: *J. Alloys Compd.*, 2017, vol. 705, pp. 756–63.
10. G. Laplanche, A. Kostka, C. Reinhart, J. Hunfeld, G. Eggeler, and E.P. George: *Acta Mater.*, 2017, vol. 128, pp. 292–303.
11. F. Otto, A. Dlouhý, C. Somsen, H. Bei, G. Eggeler, and E.P. George: *Acta Mater.*, 2013, vol. 61 (15), pp. 5743–55.
12. Z. Wu, H. Bei, G.M. Pharr, and E.P. George: *Acta Mater.*, 2014, vol. 81, pp. 428–41.
13. A. Gali and E.P. George: *Intermetallics*, 2013, vol. 39, pp. 74–8.
14. Z. Wu, H. Bei, F. Otto, G.M. Pharr, and E.P. George: *Intermetallics*, 2014, vol. 46, pp. 131–40.
15. F. Otto, N.L. Hanold, and E.P. George: *Intermetallics*, 2014, vol. 54, pp. 39–48.
16. B. Gludovatz, E. George, and R. Ritchie: *JOM-US*, 2015, vol. 67 (10), pp. 2262–70.
17. G. Laplanche, O. Horst, F. Otto, G. Eggeler, and E.P. George: *J. Alloys Compd.*, 2015, vol. 647, pp. 548–57.
18. G. Laplanche, P. Gadaud, O. Horst, F. Otto, G. Eggeler, and E.P. George: *J. Alloys Compd.*, 2015, vol. 623, pp. 348–53.
19. B. Gludovatz, A. Hohenwarter, K.V.S. Thurston, H. Bei, Z. Wu, E.P. George, and R.O. Ritchie: *Nat. Commun.*, 2016, vol. 7.
20. Z. Zhang, M.M. Mao, J. Wang, B. Gludovatz, Z. Zhang, S.X. Mao, E.P. George, Q. Yu, and R.O. Ritchie: *Nat. Commun.*, 2015, vol. 6.
21. B. Gludovatz, A. Hohenwarter, D. Catoor, E.H. Chang, E.P. George, and R.O. Ritchie: *Science*, 2014, vol. 345 (6201), pp. 1153–58.
22. M. Laurent-Brocq, A. Akhatova, L. Perrière, S. Chebini, X. Sauvage, E. Leroy, and Y. Champion: *Acta Mater.*, 2015, vol. 88, pp. 355–65.
23. M. Laurent-Brocq, L. Perrière, R. Pirès, and Y. Champion: *Mater. Design*, 2016, vol. 103, pp. 84–89.
24. Z. Wang, S. Guo, and C.T. Liu: *JOM-US*, 2014, vol. 66 (10), pp. 1966–72.
25. Z. Wang, Y. Huang, Y. Yang, J. Wang, and C.T. Liu: *Scripta Mater.*, 2015, vol. 94, pp. 28–31.
26. Y. Lu, Y. Dong, S. Guo, L. Jiang, H. Kang, T. Wang, B. Wen, Z. Wang, J. Jie, Z. Cao, H. Ruan and T. Li: *Sci. Rep.-UK*, 2014, vol. 4, pp. 6200.
27. Y. Lu, X. Gao, L. Jiang, Z. Chen, T. Wang, J. Jie, H. Kang, Y. Zhang, S. Guo, H. Ruan, Y. Zhao, Z. Cao, and T. Li: *Acta Mater.*, 2017, vol. 124, pp. 143–50.
28. M.M. Guzowski, G.K. Sigworth, and D.A. Sentner: *Metall. Trans. A*, 1987, vol. 18A, pp. 603–19.
29. Z.P. Lu, H. Wang, M.W. Chen, I. Baker, J.W. Yeh, C.T. Liu, and T.G. Nieh: *Intermetallics*, 2015, vol. 66, pp. 67–76.
30. W.H. Liu, Y. Wu, J.Y. He, T.G. Nieh, and Z.P. Lu: *Scripta Mater.*, 2013, vol. 68 (7), pp. 526–29.
31. M. Asta, C. Beckermann, A. Karma, W. Kurz, R. Napolitano, M. Plapp, G. Purdy, M. Rappaz, and R. Trivedi: *Acta Mater.*, 2009, vol. 57 (4), pp. 941–71.
32. M. Easton and D. StJohn: *Metall. Mater. Trans. A*, 1999, vol. 30A, pp. 1613–23.
33. T.T. Cheng: *Intermetallics*, 2000, vol. 8 (1), pp. 29–37.
34. N.D. Stepanov, N.Y. Yurchenko, M.A. Tikhonovsky, and G.A. Salishchev: *J. Alloys Compd.*, 2016, vol. 687, pp. 59–71.
35. S. Praveen, J. Basu, S. Kashyap, and R.S. Kottada: *J. Alloys Compd.*, 2016, vol. 662 (Supplement C), pp. 361–67.
36. Y. Shan, X. Luo, X. Hu, and S. Liu: *J. Mater. Sci. Technol.*, 2011, vol. 27 (4), pp. 352–58.
37. M.A. Easton and D.H. Stjohn: *Int. J. Cast Metal. Res.*, 2000, vol. 12(6), pp. 393–408.
38. F. Otto, A. Dlouhý, K.G. Pradeep, M. Kuběnová, D. Raabe, G. Eggeler, and E.P. George: *Acta Mater.*, 2016, vol. 112, pp. 40–52.
39. R. Günther, C. Hartig, and R. Bormann: *Acta Mater.*, 2006, vol. 54 (20), pp. 5591–97.

40. D. Shu, B. Sun, J. Mi, and P.S. Grant: *Acta Mater.*, 2011, vol. 59 (5), pp. 2135–44.
41. A.L. Greer, A.M. Bunn, A. Tronche, P.V. Evans, and D.J. Bristow: *Acta Mater.*, 2000, vol. 48 (11), pp. 2823–35.
42. L. Lu, A.K. Dahle, and D.H. StJohn: *Scripta Mater.*, 2005, vol. 53 (5), pp. 517–22.
43. S. Liu, Y. Chen, and H. Han: *J. Alloys Compd.*, 2015, vol. 624, pp. 266–69.
44. C. Tong, Y. Chen, J. Yeh, S. Lin, S. Chen, T. Shun, C. Tsau, and S. Chang: *Metall. Mater. Trans. A*, 2005, vol. 36A, pp. 881–93.
45. M. Abdel-Reihim, N. Hess, W. Reif, and M.E.J. Birch: *J. Mater. Sci.*, 1987, vol. 22 (1), pp. 213–18.
46. M. Easton and D. StJohn: *Metall. Mater. Trans. A*, 1999, vol. 30A, pp. 1625–33.
47. Y.C. Lee, A.K. Dahle, and D.H. StJohn: *Metall. Mater. Trans. A*, 2000, vol. 31A, pp. 2895–906.
48. I. Maxwell and A. Hellawell: *Acta Metall.*, 1975, vol. 23 (2), pp. 229–37.
49. K. Yamanaka, M. Mori, and A. Chiba: *Mater. Lett.*, 2014, vol. 116, pp. 82–85.